4=32

# RADIO SCIENCE

Volume 37 Number 1 January-February 2002

*Published by*
*American Geophysical Union*
*Cosponsored by*
*International Union of Radio Sciences*

U.R.S.I.

# RADIO SCIENCE

Published by American Geophysical Union

and cosponsored by International Union of Radio Science



*Radio Science* welcomes original scientific contributions on all aspects of electromagnetic phenomena related to physical problems. The coverage embraces the propagation through and interaction of electromagnetic waves with geophysical media, biological media, plasmas, and man-made structures, and includes, but is not limited to, the application of electromagnetic techniques to remote sensing of the Earth and its environment, telecommunications, signals and systems, the ionosphere, and radio astronomy. All frequencies (including optical) are of interest.

**Manuscript submission.** Please submit your manuscript electronically by logging to http://radioscience-submit.agu.org and following the instructions. For the peer-review process you may submit text in Microsoft Word, Corel Word Perfect, LaTex, or PDF; artwork should be submitted as encapsulated postscript (.eps), tagged information file format (.tif), or PDF files. See http://www.agu.org/pubs/inf4aus.html for information about file preparation.

If you have difficulties submitting electronically, please contact Kristine Pumphrey at telephone: (202) 777-7378, e-mail: kpumphrey@agu.org. Manuscript submissions should be accompanied by a statement from the corresponding author affirming that (1) all authors listed on manuscripts are aware of the submission to this journal and (2) this manuscript has not been published previously nor is under consideration by another journal. It is unethical for an author to publish manuscripts describing essentially the same research in more than one journal of primary publication. Submitting the same manuscript to more than one journal concurrently is unethical and unacceptable.

**For assistance with accepted manuscripts** or AGU publication policy, contact the Production Coordinator Kelly Levy, telephone: (202) 777-7379, e-mail: klevy@agu.org.



**Publication Charge.** For articles typeset by AGU the charge is $155 per printed page. AGU will key only those articles for which the AGU-typeset rate is paid. If the author provides electronic files, prepared according to AGU specifications, the publication charge is $75 per printed page. Authors honoring publication charges receive 100 reprints.

Owing to the rapid growth in the number of pages published in AGU journals, a page charge policy has been established to reduce the average length of papers. Authors submitting papers to *Radio Science* will be charged an additional fee of $60 for each page after page 10. The surcharge will be billed in addition to current page charges and regardless of whether reprints are ordered.

**Supplementary Material.** Data and other material supplementing journal articles or data described in a printed summary may be made available through videotape, electronic mechanisms, or microfiche. Examples include lengthy mathematical derivations, data tables, computer files, appendices, or videotaped animation. Such material will be subjected to the same peer review procedures used for printed articles. Information on retrieval and nominal handling charges will appear with the printed article or summary. For further information, contact the production coordinator.

**Subscriptions.** AGU members may subscribe to *Radio Science* in printed, online, or microfiche editions for their personal use at an annual rate of $76 for print only and $86 for print plus elelctronic subscriptions (U.S. members). Student members may subscribe at reduced rates. Subscriptions for libraries, reading rooms, and other multiple-use institutions are available at special rates; contact AGU for details. Individual nonmembers interested in subscribing to *Radio Science* for their personal use should contact AGU for information. Single-issue prices are available on request. Subscriptions and orders for back issues should be sent to: American Geophysical Union, 2000 Florida Avenue, N.W., Washington, DC 20009 USA. Fax: 202-328-0566.

**Address Changes.** Send address changes to AGU Customer Service Department with at least 5 weeks' advance notice. Claims for missing issues due to insufficient notice of address change or such reasons as "missing from files" cannot be serviced. For the U.S., lost mail should be reported within 90 days of the last day of month of publication; for other countries, within 150 days.



*Radio Science* (USPS 4539-80, ISSN 0048-6604) is published bi-monthly for $76 per year, by the American Geophysical Union, 2000 Florida Avenue, N.W., Washington, DC 20009 USA. Periodical postage paid at Washington, DC, and at additional mailing offices. POSTMASTER: Send address changes to *Radio Science*, American Geophysical Union, 2000 Florida Avenue, N.W., Washington, DC 20009 USA. RADSCAD 37(1) 1265-1880 (92001)

ISSN 0048-6604.

RADIO SCIENCE Volume 37, Number 1 January–February 2002

AGU has implemented a new pagination and citation system for all journals beginning 1 January 2002. The first number is the order in which the article appears in this printed issue. The second number is the first or last page of that article. Articles are numbered consecutively within themselves.

# Contents



*(continued on inside back cover)*

*(continued from outside back cover)*



**Author and DOI Indices follow page 16-11**

# Two-scale models for rough surface scattering: Comparison between the boundary perturbation method and the integral equation method

David Lemaire, Piotr Sobieski, Christophe Craeye, and Albert Guissard
Université catholique de Louvain, Louvain-la-Neuve, Belgium

Received 22 December 1999; revised 6 April 2001; accepted 31 July 2001; published 1 January 2002.

[1] This paper presents a comparison between two models for rough surface scattering computations: the boundary perturbation method (BPM) and the integral equation method (IEM). They differ in two fundamental aspects: the method used to compute the electric and magnetic fields on the surface and the surface information required for the computation. The two approaches lead analytically to the same solution in the two asymptotic cases of very large and very small vertical displacements, with no intermediate scales. For a composite surface the solution of the BPM is expressed as the sum of two terms, while a series development up to higher orders can be formulated with the IEM. In this paper, the comparison is restricted to composite surfaces and, particularly, to the ocean surface. After presenting a method for the two-scale decomposition of a rough surface, which satisfies the constraints of the electromagnetic model for each scale, we compute the scattering by the ocean surface using both models for various instrumental configurations and surface conditions. We show that considering the accuracy of usual radar measurements and under the assumptions made for the development of the models, both methods give very similar results. Since the BPM is based on a simple physical argument and appears to be more efficient than the two-scale IEM with regard to the computation time, the BPM should be preferred for ocean-like rough surfaces. *INDEX TERMS:* 0659 Electromagnetics: Random media and rough surfaces; 0669 Electromagnetics: Scattering and diffraction; 4275 Oceanography: General: Remote sensing and electromagnetic processes (0689); 6969 Radio Science: Remote sensing; *KEYWORDS:* radar, sea surface, scattering, boundary perturbation method, integral equation method

## 1. Introduction

[2] Radar probing of the Earth's surface has now been in use for a long time. Several Earth observation missions have already proven radar potentialities, with numerous scientific and operational products being distributed. Microwave and millimeter wave instruments present the major advantage of being able to sense the Earth's surface through cloud cover. Their main drawback compared to optical or infrared sensors is their weak spatial resolution due to the longer electromagnetic wavelength they use. This problem can be overcome using synthetic aperture techniques, leading, however, to particular disturbing effects such as speckle, target displacements, etc...


0048-6604/02/1999RS002311$11.00

[3] Radar echoes are directly related to the scattering properties of the observed scenes. Therefore a number of methods have been developed for scattering simulations and for the retrieval of geophysical parameters from microwave measurements. Among these models, empirical and theoretical ones should be distinguished. Though the first ones are usually very efficient considering their computation time, they do not allow a full understanding of the physical processes implied. Physically based theoretical models, on the other hand, allow the analysis of the sensitivity of the scattering characteristics to both target parameters and radar technical specifications. Moreover, being tabulated for particular instrumental configurations or implemented on high-performing recent computers, they can also be used as the basis for inversion algorithms for operational systems. Finally, when proven efficient, theoretical models could also be used as references for the intercalibration of multichannel active and passive instruments.

[4] Since the basic work of *Rice* [1951], an abundant literature has covered the subject of random rough surface scattering, both for the scalar case (acoustics) and for the vector case (electromagnetics), under either extreme boundary conditions (soft and hard surfaces, or perfectly conducting surfaces) or more general conditions. Extensive lists of references are to be found in some recent textbooks, e.g., those by *Fung* [1994] or *Voronovitch* [1994]. Among all proposed methods, two-scale methods work rather well for the case of the ocean surface, because the separation between the large-scale component and the small-scale component is somehow related to gravity and capillary waves. We have developed a two-scale approach [*Guissard and Sobieski*, 1987; *Guissard et al.*, 1992], based on the boundary perturbation method (BPM) [*Burrows*, 1973]. It leads to numerical results that compare rather well with experimental data [*Lemaire et al.*, 1999]. Another method that has encountered a large audience in recent years is the integral equation method (IEM) proposed by *Fung et al.* [1992] and *Fung* [1994], which can be applied for both ocean and soil surfaces.

[5] We present in this paper a comparison between these two theoretical models for rough-surface-scattering computation. Since both methods lead to the same asymptotic solution in the cases of either very small vertical displacements of the surface with small slopes or very large surface displacements with large curvature radii, we shall focus on the case of a composite surface where different scales of roughness may be present. In section 2, the two models are presented following a scheme of increasing complexity, so that it remains as clear as possible and facilitates the following discussions. The presentation is restricted to the main steps that highlight the differences between the methods, and the reader is referred to the literature whenever the mathematical developments are not relevant to the purpose of this paper. Next, the results obtained with both methods are compared in the case of the ocean surface and for various radar configurations. Since the solution appears as a series development for both methods, we analyze the results starting with the zeroth-order term and then continuing with higher-order terms.

## 2. Rough-Surface-Scattering Models

[6] A usual quantity derived from the radar echo measurements is the normalized radar cross section (NRCS) or scattering coefficient $\sigma^o$. Consider a rough surface $z = \zeta(x, y)$, horizontal in the mean. A portion of the surface with horizontal area $A$ is illuminated by a plane wave $\mathbf{E}_p^i = E_0\mathbf{p}e^{(-jk\mathbf{i}\cdot\mathbf{r})}$ from direction $\mathbf{i}$ and polarization $\mathbf{p}$. It induces a scattered field $\mathbf{E}_q^s$ with polarization $\mathbf{q}$ into the direction $\mathbf{s}$. The bistatic scattering coefficient is then defined as

$$\sigma_{pq}^o(\mathbf{i}, \mathbf{s}) = \frac{4\pi R^2}{A}\frac{|\mathbf{E}_q^s|^2}{|\mathbf{E}_p^i|^2}, \tag{1}$$

where $R$ stands for the observation distance.

[7] The time dependence $e^{j\omega t}$ being understood, the scattered field $\mathbf{E}^s$, at large distance from the target, can be evaluated from the knowledge of the induced electric and magnetic surface fields $\mathbf{E}$ and $\mathbf{H}$, by

$$\mathbf{E}^s = -jk\frac{e^{-jkR}}{4\pi R}\mathbf{s} \times \iint_S [\mathbf{n} \times \mathbf{E} - \mathbf{s} \times (\mathbf{n} \times \eta\mathbf{H})]e^{-jk\mathbf{s}\cdot\mathbf{r}}dS, \tag{2}$$

where $\mathbf{r}$ represents a point of the surface $S$, $\mathbf{n}$ is the normal to the surface at that point, and $k$ is the electromagnetic wave number.

[8] For a rough surface, $\mathbf{r}$, $\mathbf{n}$, $\mathbf{E}$, and $\mathbf{H}$ are stochastic functions of time and position. Since the measurement of radar echoes from a rough surface proceeds by averaging a large number of independent return pulses, each of them being the combination of echoes produced by a large amount of individual scatterers, one defines the total scattering coefficient associated with the total field as follows (the angle brackets denoting an ensemble average):

$$\sigma_{pq}^o(\mathbf{i}, \mathbf{s}) = \frac{4\pi R^2}{A}\frac{< |\mathbf{E}_q^s|^2 >}{|\mathbf{E}_p^i|^2}. \tag{3}$$

[9] We follow hereafter the scheme presented by *Guissard* [1996]. We normalize the surface fields with respect to the incident electric field,

$$\mathbf{E}(\mathbf{r}) = E_0\mathbf{e}_p(\mathbf{r})e^{(-jk\mathbf{i}\cdot\mathbf{r})}, \quad \mathbf{H}(\mathbf{r}) = \frac{1}{\eta}E_0\mathbf{h}_p(\mathbf{r})e^{(-jk\mathbf{i}\cdot\mathbf{r})}, \tag{4}$$

with $\eta$ the intrinsic impedance of the propagation medium, and we extract the component of the scattered field with polarization $\mathbf{q}$, i.e., $E_q^s = \mathbf{q} \cdot \mathbf{E}^s$. The total bistatic scattering coefficient $\sigma_{pq}^o$ can be evaluated by

$$\sigma_{pq}^o(\mathbf{i}, \mathbf{s}) = \frac{k^2}{4\pi A}\iint_S\iint_S < S_{pq} \exp\left[j\mathbf{v}\cdot(\mathbf{r}' - \mathbf{r}'')\right] > dx'dy'dx''dy'', \tag{5}$$

where $\mathbf{r}' = (x', y', \zeta')$ and $\mathbf{r}'' = (x'', y'', \zeta'')$ are two points on the surface, $\mathbf{v} = k(\mathbf{s} - \mathbf{i})$, and $S_{pq}$ is given by

$$S_{pq} = \frac{F_{pq}(\mathbf{r}')F_{pq}^*(\mathbf{r}'')}{(\mathbf{n}'\cdot\mathbf{z})(\mathbf{n}''\cdot\mathbf{z})}, \tag{6}$$

with

$$F_{pq}(\mathbf{r}) = \mathbf{s} \times [\mathbf{n} \times \mathbf{e}_p - \mathbf{s} \times (\mathbf{n} \times \mathbf{h}_p)] \cdot \mathbf{q} \qquad (7)$$

and the asterisk indicating the complex conjugate. In expression (6), $z$ is the unit vertical vector, and $\mathbf{n}'$ and $\mathbf{n}''$ are the unit vectors normal to the surface at $\mathbf{r}'$ and $\mathbf{r}''$, respectively. In (7) the field vectors $\mathbf{e}_p$ and $\mathbf{h}_p$ and the unit vector $\mathbf{n}$ normal to the surface must be evaluated at the location $\mathbf{r}$ on the surface.

[10] In the above relations, $\zeta' = \zeta(x', y')$ and $\zeta'' = \zeta(x'', y'')$ represent the elevation of the surface above the horizontal plane of reference. They are stochastic functions of the horizontal coordinates of $\mathbf{r}'$ and $\mathbf{r}''$. Under the assumption of spatial stationarity the averaged quantity in (5) only depends on the difference in position $\mathbf{r} = (\mathbf{r}' - \mathbf{r}'')$. Further, if the correlation length of this random quantity is small compared to the dimensions of the area $A$, (5) may be simplified as follows [*Ulaby et al.*, 1982, volume 2, chapter 12]:

$$\sigma^o_{pq} = \frac{k^2}{4\pi} \int\int_S < S_{pq} e^{[jv_z(\zeta' - \zeta'')]} > \exp[jv_x x + jv_y y] dx dy, \qquad (8)$$

where $\mathbf{v} \cdot \mathbf{r} = v_z(\zeta' - \zeta'') + v_x x + v_y y$ has been used.

[11] In the expression above, the surface field term $S_{pq}$ and the phase term $e^{[jv_z(\zeta' - \zeta'')]}$ are both difficult to evaluate. Existing methods are based on different sets of assumptions. First, the ensemble average involves the product of two factors. The exponential term only depends on the vertical displacement, while $S_{pq}$ is a function of the shape of the surface, i.e., of the slopes, curvatures, etc.... It can be shown, furthermore, that under the assumption of spatial stationarity the displacement at one point of the surface is not correlated with the slopes at that point. In the particular case of Gaussian surface statistics this implies that these variables are independent. Although the same argument does not apply to two separate points, we shall assume that the ensemble average may be factorized as

$$< S_{pq} e^{[jv_z(\zeta' - \zeta'')]} > = < S_{pq} >_{\text{shape}} < e^{[jv_z(\zeta' - \zeta'')]} >_{\text{displ}} . \qquad (9)$$

[12] It must be stressed that in certain derivations this assumption is not necessary or is simply induced, because of the set of initial assumptions (for instance, *under the small-slopes assumption, the* $S_{pq}$ term is usually slope-independent, hence position-independent too). The product factorization in (9) is based on a heuristic argument and does not ensure a correct solution. The proof of its validity can only be obtained a posteriori, showing that it leads to a good approximation of the reality. This factorization is made explicitely in the BPM and implicitly in the IEM.

[13] The second factor of (9) can be identified as the joint characteristic function $\chi_2$ of the displacements at two points, evaluated at $(v_z, -v_z)$. If the surface dimensions are large compared to the correlation length of the variables over which the ensemble averages are taken, the limits of integration may be extended to infinity, and we obtain

$$\sigma^o_{pq} = \frac{k^2}{4\pi} \int\int_{-\infty}^{\infty} < S_{pq} > \chi_2(v_z, -v_z) \times \exp(jv_x x + jv_y y) dx\, dy. \qquad (10)$$

[14] For the particular case of a normal surface the joint probability density function (pdf) of the vertical displacements at two points is a Gaussian function, and we have

$$\chi_2(v_z, -v_z) = \exp\{-\sigma^2 v_z^2 [1 - C(\rho)]\}, \qquad (11)$$

where $C(\rho)$ is the autocorrelation function of surface heights and $\rho = (x, y)$ denotes a position in the horizontal plane of reference. When the joint pdf of the vertical displacements is not Gaussian, the expression of $\chi_2$ becomes more complicated. The analysis of this case is given by *Guissard* [1996]. It yields $\sigma^o_{pq}$ components whose evaluation requires high-order statistics (bicovariance, bispectrum, etc.) of the surface displacements. In the following analysis, we assume that relation (11) is valid.

[15] To make the following discussion as clear as possible, we shall recall hereafter the results in the two asymptotic cases of very large and very small surface displacements compared to the electromagnetic wavelength.

### 2.1. Very Large Displacements

[16] In the first case, $k\sigma$ is assumed very large. *Ulaby et al.*, [1982, volume 2, chapter 12] express the limit of validity as

$$k\sigma > \sqrt{10}. \qquad (12)$$

[17] The characteristic function (11) has then negligible values except in the vicinity of origin where $C(0,0) = 1$. Assuming, in addition, that the curvature radii are large compared to the electromagnetic (EM) wavelength, the Kirchhoff's approximation can be used for the evaluation of $S_{pq}$. Expanding the correlation function $C(x, y)$ around the origin, the integration can be performed, and the well-

known physical optics solution is found [*Guissard et al.*, 1992]:

$$\sigma^o_{pq} = \frac{\pi}{\cos^4\gamma_{sp}} |R_{pq}(\mathbf{n}_{sp})|^2 T(-\frac{v_x}{v_z}, -\frac{v_y}{v_z}). \qquad (13)$$

where the Fresnel coefficient $R_{pq}(\mathbf{n}_{sp})$ is evaluated on a plane oriented so that $\mathbf{s}$ and $\mathbf{i}$ correspond to a specular reflection, while the slope probability density function $T$ is evaluated for the values $(-v_x/v_z, -v_y/v_z)$ leading to a tangent plane with such an orientation. Here, $\mathbf{n}_{sp}$ is the normal to the surface at these specular points, and $\gamma_{sp}$ is the angle between this normal and the vertical, i.e., $\cos\gamma_{sp} = \mathbf{n}_{sp} \cdot \mathbf{z}$.

### 2.2. Very Small Displacements

[18] For very small surface displacements the small perturbation method (SPM) [*Rice*, 1951] applies. The result can be directly obtained from (10) using a much simpler derivation. With the assumption of small slopes, the normal $\mathbf{n}$ to the surface is close to the vertical $\mathbf{z}$, and we can use the approximation $\mathbf{n} \cdot \mathbf{z} \approx 1$. To the first order, we have

$$F_{pq}(\mathbf{r}) \approx F_{pq}\big|_{\mathbf{n}=\mathbf{z}}, \qquad < S_{pq} > \approx \big|F_{pq}\big|^2_{\mathbf{n}=\mathbf{z}}. \qquad (14)$$

Assuming a Gaussian joint pdf of the surface displacements at two points, $\chi_2$ can be written as (11), and using a series expansion of the exponential, it can also be expressed as

$$\exp\{-\sigma^2 v_z^2[1 - C(\rho)]\} = e^{(-\sigma^2 v_z^2)}\left\{1 + \sum_{n=1}^{\infty} \frac{[\sigma^2 v_z^2 C(\rho)]}{n!}\right\}. \qquad (15)$$

With the small displacement assumption, $k\sigma \ll 1$, $\chi_2$ simplifies to the first order as

$$\chi_2(v_z, -v_z) = 1 - \sigma^2 v_z^2 + \sigma^2 v_z^2 C(\rho). \qquad (16)$$

and we get

$$\sigma^o_{pq} = \frac{k^2}{4\pi} \big|F_{pq}\big|^2_{\mathbf{n}=\mathbf{z}} [4\pi^2(1-\sigma^2 v_z^2)\delta(v_x)\delta(v_y) + v_z^2 \gamma(v_x, v_y)]. \qquad (17)$$

where $\delta$ represents the Dirac function. Here, $\gamma(\mathbf{K})$ is the surface vertical displacement spectrum, i.e., the Fourier transform of the autocovariance function $\Gamma(x, y) = \sigma^2 C(x, y)$,

$$\gamma(\mathbf{K}) = \int\int_{-\infty}^{\infty} \Gamma(x,y) \exp[jK_x x + jK_y y] dx\, dy \qquad (18)$$

taken at the Fourier components $K_x = v_x$ and $K_y = v_y$. The function $|F_{pq}|_{\mathbf{n} = \mathbf{z}}^2$ in (17) can be evaluated with the boundary perturbation method (BPM) [*Burrows*, 1967], which is equivalent to the SPM for the first-order term as proved by *Craeye et al.* [2000], with the result that

$$\big|F_{pq}\big|_{\mathbf{n}=\mathbf{z}} = 4\frac{k}{v_z} \cos\theta_i \cos\theta_s \big|\alpha_{pq}\big|, \qquad (19)$$

where $\theta_i$ and $\theta_s$ stand for the incidence and scattering off-nadir angles and an expression of the $\alpha_{pq}$ is given, for instance, by *Ruck et al.* [1970]. (The same coefficients are also given by *Ulaby et al.*, [1982, volume 2], with sign errors, however.) In the specular direction, i.e., for $v_x = v_y = 0$, relation (19) reduces to

$$\big|F_{pq}\big|_{n=z} = 2\cos\theta_i \big|R_{pq}(\theta_i)\big|. \qquad (20)$$

Finally, the total bistatic scattering coefficient is given by

$$\sigma^o_{pq} = 4\pi k^2 \cos^2\theta_i \big|R_{\text{eff}.\,pq}(\theta_i)\big|^2 \delta(v_x)\delta(v_y) + 4\frac{k^4}{\pi} \cos^2\theta_i \cos^2\theta_s \big|\alpha_{pq}\big|^2 \gamma(v_x, v_y), \qquad (21)$$

where $|R_{\text{eff}.\,pq}|^2 = (1 - \sigma^2 v_z^2)\, |R_{pq}|^2$ denotes an effective Fresnel coefficient, taking into account the decrease of the power in the specular direction due to the scattering of the incident wave in all directions by the surface ripples.

[19] In (21) the total scattering coefficient appears as the sum of two terms. The first term corresponds to the coherent scattering coefficient, defined as

$$\sigma^{oc}_{pq}(\mathbf{i}, \mathbf{s}) = \frac{4\pi R^2}{A} \frac{| < \mathbf{E}^s_q > |^2}{|\mathbf{E}^i_p|^2}, \qquad (22)$$

and becomes negligible as the ratio between the surface roughness and the electromagnetic wavelength increases. The second term corresponds to the incoherent scattering coefficient. It is commonly referred to as the Bragg scattering mechanism, since it shows that the scattering results from the components of the spectrum $v_x$ and $v_y$ that produce a constructive interference in the scattering direction.

[20] The same result can be obtained using the integral equation method (IEM) to obtain an expression of the field coefficient $S_{pq}$ in (10) [*Fung*, 1994, chapter 4]. An advantage of this method is that it provides also an expression of the scattering coefficient when the development of $\chi_2$ in (15) is not limited to the first order, yielding then an improved accuracy when $k\sigma$ is not negligible compared to unity. A complete expression in this case is given by *Fung* [1994].

### 2.3. Composite Surface

[21] For natural targets such as the ocean, for instance, the surface is composed of many scales of roughness. In this case, the physical optics and the Bragg solutions apply strictly to millimeter waves and HF waves, respectively. The IEM can yield a better solution over a larger range of wavelengths when enough terms of the series expansion (15) are used; however, it becomes practically inapplicable when too many terms must be computed. We present hereafter two methods for the computation of the scattering by a composite surface. One is based on a boundary perturbation approach and is developed by *Guissard et al.* [1992]; the other is an extension of the integral equation approach for the case of a composite surface. We briefly recall the main assumptions of the BPM and present the developments for the two-scale extension of the IEM. These two methods are numerically compared in sections 3 and 4.

[22] In order to develop a simple and efficient method, *Guissard et al.* [1992] extended the boundary perturbation method initially proposed by *Burrows* [1967, 1973] and *Brown* [1978] to bistatic scattering by a dielectric rough interface. In this method, it is assumed that the surface is composed of the superposition of small ripples with RMS value $\sigma_R$ such that $k\sigma_R \ll 1$ on large waves with RMS vertical displacements $\sigma_L$. The two surface components are assumed to be independent stochastic processes, and their corresponding spectrum is computed by splitting the spectrum of the composite surface $\gamma(\mathbf{K})$ at a given wave number $K_{\lim}$, such that the large-scale spectrum $\gamma_L$ and the small-scale spectrum $\gamma_R$ satisfy

$$\begin{aligned}
\gamma_L(K_x, K_y) &= \gamma(K_x, K_y) \quad \sqrt{K_x^2 + K_y^2} \le K_{\lim}, \\
\gamma_R(K_x, K_y) &= \gamma(K_x, K_y) \quad \sqrt{K_x^2 + K_y^2} > K_{\lim}, \\
\sigma_L &= \sqrt{\frac{1}{4\pi^2}\int_0^{K_{\lim}}\int_0^{2\pi}\gamma_L(K,\alpha)KdKd\alpha} \quad k\sigma_L \gg 1, \\
\sigma_R &= \sqrt{\frac{1}{4\pi^2}\int_{K_{\lim}}^{\infty}\int_0^{2\pi}\gamma_R(K,\alpha)KdKd\alpha} \quad k\sigma_R \ll 1,
\end{aligned} \tag{23}$$

where a cylindrical coordinate system such that $(K_x, K_y)$ = $(K \cos \alpha, K \sin \alpha)$ has been assumed for the last two relations.

[23] The total scattered field is then expressed as an expansion with respect to $\sigma_R$,

$$\mathbf{E}_q^s = \mathbf{E}_{q0}^s + \mathbf{E}_{q1}^s + \cdots \tag{24}$$

The zeroth-order term is the solution for the field scattered by the large-scale component without ripples. Assuming large curvature radii $\rho_L$ for the large scale, Kirchhoff's approximation can be used to determine it. Next, assuming constant values of the zeroth-order electromagnetic fields inside the volumes determined by the small waves, the perturbation field at large distance from the surface $\mathbf{E}_{q1}^s$ due to the ripples is evaluated. Finally, removing the cross term $2\,Re\langle\mathbf{E}_{q0}^s\cdot\mathbf{E}_{q1}^{s*}\rangle$ in the evaluation of $\langle|\mathbf{E}_q^s|^2\rangle$, thanks to the assumption of independence between large and small roughness scales, the scattering coefficient is expressed as the sum of two terms:

$$\sigma_{pq}^o = \sigma_{pq0}^o + \sigma_{pq1}^o. \tag{25}$$

The zeroth-order term is given by the Kirchhoff solution for the large-scale surface (13) with the Fresnel coefficient $R_{pq}$ replaced by an effective Fresnel coefficient $R_{\mathrm{eff},pq}$ similarly to (21). This latter takes into account the effect of the ripples present on the "tangent planes" on the large waves as

$$R_{\mathrm{eff},pq} = e^{[-(1/2)\sigma_R^2 v_z^2]}R_{pq}. \tag{26}$$

On the other hand, the expression of the first-order term is

$$\sigma_{pq1}^o = \frac{k^2}{4\pi(v_z/k)^2}\iint_{-\infty}^{\infty} |H_{PQ}(\alpha,\beta)|^2\gamma_R(K_x,K_y)T_{sl}(\alpha,\beta)d\alpha d\beta, \tag{27}$$

where

$$\alpha = -\frac{v_x - K_x}{v_z}, \beta = -\frac{v_y - K_y}{v_z}. \tag{28}$$

[24] $T_{sl}(\alpha, \beta)$ corresponds to the large-scale slope pdf, and the expression of the surface field function $H_{PQ}$ is given by *Guissard et al.* [1992]. Analyzing this expression closely, we note that as for the incoherent term of (21), the scattering results from the Fourier components of the surface spectrum that produce a constructive interference in the scattering direction. The difference with (21) is that, since in this case the ripples lie on large tilting undulations (with a certain probability density $T_{sl}(\alpha, \beta)$), a certain range of Fourier components may have the correct wavelength and orientation to yield a constructive interference. This results in the convolution between the ripple spectrum $\gamma_R$ and the large-scale slope probability density function $T_{sl}$. Moreover, the $H_{PQ}(\alpha, \beta)$ function has also been shown by *Craeye et al.* [2000] to be identical to the $\alpha_{pq}$ in (21), and therefore we sometimes refer to expression (27) as "tilted Bragg" solution hereafter. In particular, when only ripples are present on a flat surface, $T_{sl}(\alpha, \beta)$ reduces to a product of Dirac functions and the solution degenerates into the SPM or Bragg scattering solution [*Guissard et al.*, 1989].

[25] Another approach can be followed in the case of scattering by a composite surface. It is based on a two-

scale expansion of the IEM. The detailed developments are given by *Lemaire* [1998]. We summarize them hereafter. Using the IEM, the surface fields appear as the sum of a Kirchhoff and a complementary term. The scattering coefficient appears as the sum of several terms, and each term can be factorized under a form similar to (10). If the spectrum $\gamma$ of the composite surface is expressed as the sum of a large-scale spectrum $\gamma_L$ and a small-scale spectrum $\gamma_R$ using (23), the covariance function is equal to the sum of two functions corresponding to the inverse Fourier transform of the respective spectra, i.e.,

$$\Gamma(x,y) = \Gamma_L(x,y) + \Gamma_R(x,y). \tag{29}$$

Consequently, the characteristic function (11) can be written as

$$\begin{aligned}\chi_2(v_z, -v_z) &= \exp\{-v_z^2[\sigma_L^2 - \Gamma_L(\rho)]\} \\ &\quad \times \exp\{-v_z^2[\sigma_R^2 - \Gamma_R(\rho)]\} \\ &= \chi_{2L}(v_z, -v_z)\ \chi_{2R}(v_z, -v_z).\end{aligned} \tag{30}$$

[26] Next, as done above when only one scale of roughness is present, the covariance function of the large scale can be expanded around the origin (see section 2.1), and the joint characteristic function of the small scale can be developed in series (see section 2.2). The surface fields being evaluated using the integral equation, the integration along the horizontal coordinates, can be performed. Since, similarly to (10), all terms of the scattering coefficient appear as the Fourier transform of a product of two functions $\chi_{2L}$ and $\chi_{2R}$, two partial solutions can be found in a first step by integration on the large and the small scales separately. Then, using the properties of the Fourier transform with regard to the product of two functions, the complete solution is the convolution of these partial solutions. We obtain, finally, the series expansion [*Lemaire*, 1998]

$$\sigma_{pq}^o = \sigma_{pq0}^o + \sum_{n=1}^{\infty} \sigma_{pqn}^o + \sum_{m=1}^{\infty}\sum_{n=1}^{\infty} \sigma_{pqmn}^o. \tag{31}$$

[27] As with the BPM, the zeroth-order term is given by Kirchhoff's solution for the large-scale surface (equation (13)) with an effective Fresnel coefficient $R_{\mathrm{eff},pq}$ taking into account the effect of the ripples:

$$R_{eff.\,pq} = J_{pq} \exp\left[-\frac{1}{2}\sigma_R^2 v_z^2\right] R_{pq}. \tag{32}$$

$J_{pq}$ denotes the difference with BPM and is given by

$$\begin{aligned}J_{pq} = 1 + \frac{e^{-\sigma_R^2 k_{iz} k_{sz}}}{2R_{pq}} &\left[F_{pq}(u^*, v^*) + \frac{k_{iz}k_{sz}}{4\pi^2}\right. \\ &\left.\times \int\int_{-\infty}^{\infty} F_{pq}(u^* + \alpha, v^* + \beta)\gamma_R(\alpha,\beta) d\alpha d\beta\right],\end{aligned} \tag{33}$$

where

$$u^* = \frac{k_{iz}k_{sx} - k_{sz}k_{ix}}{k_{sz} - k_{iz}},\ v^* = \frac{k_{iz}k_{sy} - k_{sz}k_{iy}}{k_{sz} - k_{iz}}, \tag{34}$$

$$\mathbf{k}_i = k\mathbf{i} = (k_{ix}, k_{iy}, k_{iz}), \qquad \mathbf{k}_s = k\mathbf{s} = (k_{sx}, k_{sy}, k_{sz}). \tag{35}$$

[28] Similarly to (27), the single scattering terms $\sigma_{pqn}{}^o$ are given by

$$\begin{aligned}\sigma_{pqn}^o &= \frac{k^2}{4\pi v_z^2} \exp\left[-\sigma_R^2 v_z^2\right] \\ &\times \int\int_{-\infty}^{\infty} |I_{pqn}(\alpha,\beta)|^2 \frac{\gamma_R^{(n)}(K_x, K_y)}{n!} T_{sl}(\alpha,\beta) d\alpha d\beta.\end{aligned} \tag{36}$$

In this expression, the $\gamma_R^{(n)}$ functions are defined as the spatial Fourier transform of the $n$th power of the ripples autocovariance function, i.e.,

$$\gamma_R^{(n)}(K_x, K_y) = FT\{\Gamma_R^n(\rho)\}. \tag{37}$$

The surface field functions $I_{pqn}$ are given by

$$\begin{aligned}I_{pqn}(\alpha,\beta) = v_z^n f_{pq} + \frac{e^{-\sigma_R^2 k_{iz} k_{sz}}}{2} &\left[k_{sz}^n F_{pq}(-k_{ix}', -k_{iy}')\right. \\ &\left. + (-k_{iz})^n F_{pq}(-k_{sx}', -k_{sy}')\right],\end{aligned} \tag{38}$$

where the expressions of the $f_{pq}$ and $F_{pq}$ factors are given by *Fung* [1994] and the wave numbers

$$\begin{aligned}k_{ix}' &= k_{ix} + k_{iz}\alpha, \\ k_{iy}' &= k_{iy} + k_{iz}\beta, \\ k_{sx}' &= k_{sx} + k_{sz}\alpha, \\ k_{sy}' &= k_{sy} + k_{sz}\beta,\end{aligned} \tag{39}$$

geometrically correspond to the local tangential wave number components on large waves, if the large-scale slopes are small compared to unity.

[29] The single-scattering terms are thus given by a convolution between the ripple spectral functions $\gamma_R^{(n)}$ and the large-scale slope probability density function. Hence, as for (27), this expression can be physically interpreted as resulting from the interaction between small waves propagating on large tilting waves. Finally, the higher-order terms $\sigma_{pqmn}^o$ take multiple scattering into account. They represent the influence of the electromagnetic fields at one point of the surface on the neighboring points. Their expression is given in Appendix A since they are quite long and complicated. They will not be considered in the following analysis.

[30] For a slightly rough surface, $T_{sl}(\alpha, \beta)$ degenerates into a product of Dirac functions. In this case, the $\sigma_{pqn}^o$

can be shown to reduce to the expressions given by *Fung* [1994, section 5.5.1], which are themselves equivalent to the SPM solution when the development is limited to the first order for small $k\sigma_R$ compared to 1. However, contrary to BPM, it is important to note that relation (36) for $n = 1$ is not equivalent to the tilted Bragg solution. Indeed, as already mentioned, when no large scale is present and when the exponential terms $\exp\{-[\sigma_R{}^2 v_z{}^2]\}$ in (36) and $\exp\{-[\sigma_R{}^2 k_{iz} k_{sz}]\}$ in (38) can be approximated to unity, the solution reduces to the SPM solution (21), as does (27). Thus, for a composite surface, not considering the exponential factors in (36) and (38), if all the wave number components in expression (38) of $I_{pqn}$ were evaluated as local wave numbers with reference to the tilting large scale, (36) would correspond like (27) to the tilted Bragg solution. However, although (39) shows that the $F_{pq}$ functions in (38) are indeed calculated for tangential wave number components ($k'_{ix}$, $k'_{iy}$, $k'_{sx}$, and $k'_{sy}$) evaluated locally, the vertical components $k_{iz}$ and $k_{sz}$ in (38) are taken with reference to the global incidence angle. Hence expression (36) of $\sigma^o_{pqn}$ with $n = 1$ does not correspond exactly to the tilted Bragg solution.

[31] This important difference is due to the fact that the integration of the various terms (similar to (10)) of the scattering coefficient is performed along the horizontal coordinates. Therefore, when a two-scale decomposition is used, the convolution is performed only on the horizontal wave number components; whereas, since $v_z$ or $k_{iz}$ and $k_{sz}$ appear only as multiplicative factors of the covariance function in the series development of $\chi_2$, no convolution is performed on the vertical components of the vectors, and they are thus evaluated in the global coordinate system. This might result from initial assumptions done to compute the surface fields using the IEM, such as the small-slopes assumption. Although it would seem more intuitive to use also vertical wave number components evaluated locally in the expression of the $I_{pqn}$ functions, we use expression (38) obtained analytically, knowing that its validity is limited to the assumptions made for the developments.

## 3. Limit Wave Number Problem

[32] In section 2, we briefly reviewed electromagnetic models for rough surface scattering. We ended with the BPM and the two-scale development of the IEM that will be compared in section 4. Different conditions were imposed on each scale for the application of the scattering models. These constraints depend on the electromagnetic wavelength (and thus on the instrumental configuration) and on the surface roughness, which is related to a number of environmental conditions for natural rough surfaces such as the ocean. Both the surface and the instrumental characteristics should therefore be taken into account to decompose the surface so that the electromagnetic constraints are satisfied. This is the purpose of this section.

[33] For the application of the two-scale models in the case of a composite surface, we split the surface into small and large waves following (23). For the large-scale component, besides the condition (23) on its vertical displacements, the curvature radius should be much larger than the electromagnetic wavelength everywhere on the surface for the Kirchhoff's approximation to be valid. For the small-scale component the surface vertical displacements need to be small compared to the electromagnetic wavelength. This was required for the BPM to assume constant fields inside the volumes determined by the small roughness; while for the two-scale expansion of the IEM, this assumption allows the use of a series expansion of the joint characteristic function of the small-scale vertical displacements.

[34] For the small scale, the condition on the displacements is given by

$$k\sigma_R \ll 1, \tag{40}$$

with $\sigma_R$ given by (23). From its definition the surface spectrum $\gamma$ is a symmetric function with respect to the origin. It is usually factorized as [*Lemaire et al.*, 1999]

$$\gamma(K,\alpha) = 4\pi^2 \frac{S(K)}{K} F(K,\alpha), \tag{41}$$

where $S(K)$ is the radial surface spectrum and $F(K, \alpha)$ represents the azimuthal variation of the spectrum and is normalized so that $\int_0^{2\pi} F(K, \alpha) d\alpha = 1$. Using this factorization, $\sigma_R$ is given by

$$\sigma_R = \sqrt{\int_{K_{lim}}^{\infty} S(K)\, dK}. \tag{42}$$

On the other hand, the constraint on the very rough surface is that the mean curvature radius is large compared to the wavelength. With $\sigma_{\rho_c}$ being the standard deviation of the curvature radius, we write it as

$$\sigma_{\rho_c} \gg \lambda. \tag{43}$$

The curvature radius at one point of a surface in a given direction is expressed as

$$\rho_c = \frac{(1+\zeta')^{3/2}}{\zeta''}. \tag{44}$$

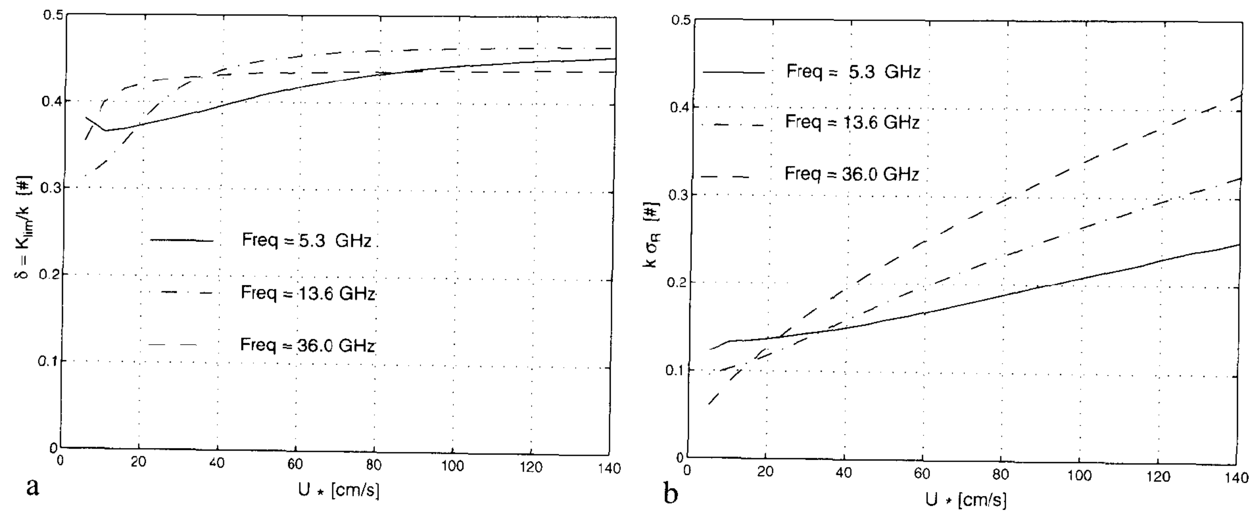


**Figure 1.** Two-scale decomposition for various frequencies. (a) Ratio $\delta = K_{\lim}/k$ and (b) $k\sigma_R$ product.

Here, $\zeta$ denotes, as mentioned in section 2, the elevation of the surface with respect to a horizontal plane of reference, and $\zeta'$ and $\zeta''$ are the first and second derivatives of $\zeta$, respectively, with respect to horizontal coordinates following the chosen direction. For small surface slopes we have

$$\rho_c \approx \frac{1}{\zeta''}. \tag{45}$$

and (43) is transformed as

$$\frac{2\pi}{k}\sigma_c \ll 1, \tag{46}$$

where $\sigma_c$ stands for the standard deviation of the surface curvature $\zeta''$. It may be estimated from the surface spectrum by

$$\sigma_c = \sqrt{\int_0^{K_{\lim}} K^4\, S(K)\, dK}. \tag{47}$$

Then, letting (40) and (46) have the same limit value to obtain a unique limit wave number, we have

$$\frac{4\pi^2}{k^2}\int_0^{K_{\lim}} K^4\, S(K)\, dK = k^2 \int_{K_{lim}}^{\infty} S(K)\, dK. \tag{48}$$

[35] We applied this relation to the case of the ocean surface. We used the surface spectrum presented by *Lemaire et al.* [1999], with 0.7% significant slope, a fetch of 500 km, and the peak wave number given by Pierson's formula for fully developed state. The ratio $\delta = K_{\lim}/k$ is plotted in Figure 1a for C, Ku, and Ka Bands. We also plot the $k\sigma_R$ product in Figure 1b. We see that $k\sigma_R$ values lie below unity as required for the small scale. As the conditions on the small and large scales have the same limit value, a small $k\sigma_R$ product also means that the curvature radius to EM wavelength ratio is large, as necessary for the large scale. We also verified that (12) is satisfied for the large scale. Finally, several authors use a constant value $\delta$ to split the spectrum into two scales. The range of values usually recommended is $0.3 < \delta < 0.5$ [*Kim and Rodriguez*, 1992]. We note from Figure 1 that the $\delta$ values computed using the proposed method lie in this recommended range.

[36] Besides the constraints on the height of the small scale and the curvature of the large scale, conditions on the correlation length of each scale have also been proposed in the literature. These conditions are usually expressed for the case of a Gaussian surface and for the asymptotic cases of the physical optics solution or the SPM solution. We verify hereafter that these conditions are satisfied by the above decomposition of the surface.

[37] Let us denote as $l_L$ and $l_R$ the correlation lengths of the large and the small scale, respectively. In the case of a Gaussian surface, imposing the constraint that the curvature radius of the large scale should be much larger than the electromagnetic wavelength, *Ulaby et al.*, [1982, volume 2, chapter 12] state that the expression of the physical optics solution, i.e., the zeroth-order term without correction of the Fresnel coefficient, should be valid if

$$k^2 l_L^2 > 2\pi\ 2.76\ k\sigma_L. \tag{49}$$

[38] For the first-order term, *Thorsos and Jackson* [1989] expressed the limit of validity of the small-

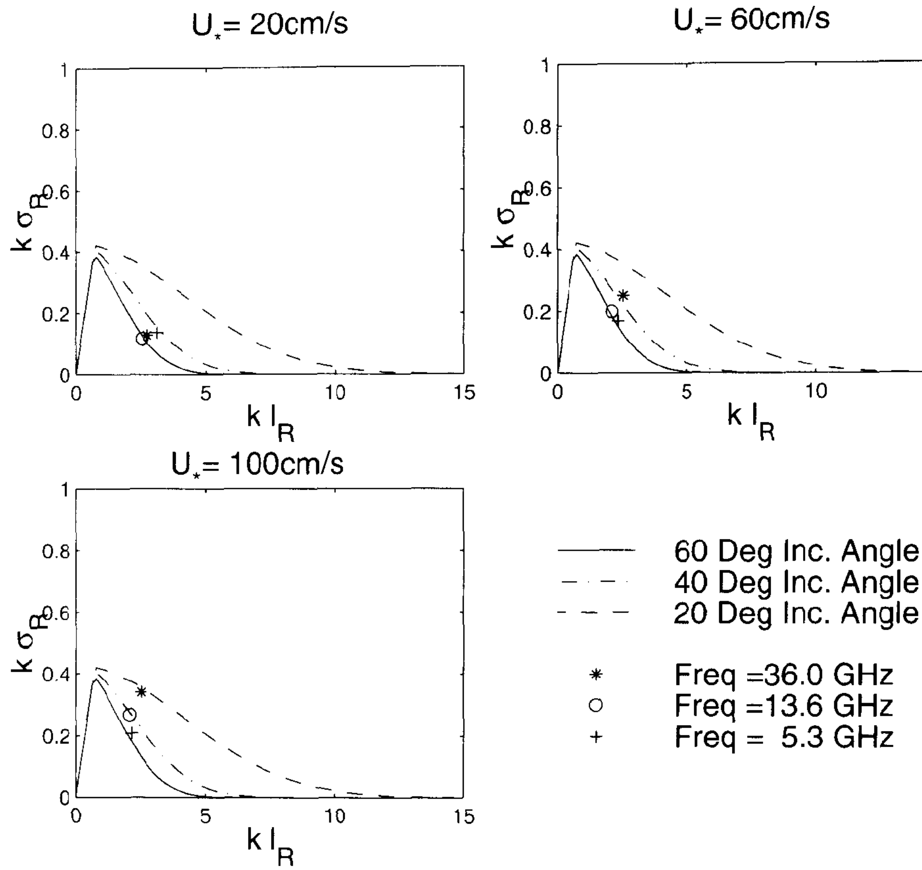


**Figure 2.** Limit of validity of the first-order term expressed by *Thorsos and Jackson* [1989] (lines) and values of the correlation length and height variance of the small scale given by our two-scale decomposition of the surface (symbols). The condition expressed by Thorsos and Jackson can be considered as satisfied.

perturbation method (i.e., the first-order term of the two-scale model, without taking the tilting of the small-scale surface by the large waves into account) as

$$\begin{aligned} &k\sigma_R < \tfrac{0.6051}{\sqrt{2}} kl_R && kl_R < B, \\ &k\sigma_R < 0.428 \exp\left[-0.25k^2 l_R^2 \sin^2\theta_i\right] && kl_R \geq B, \end{aligned} \quad (50)$$

where $B$ is a number close to unity and corresponds to the intersection of both expressions. This condition was established for the case of a one-dimensional surface with a Gaussian spectrum. Since it is not easy to conclude that this condition would remain exactly the same in the case of a two-dimensional non-Gaussian spectrum, we use it hereafter merely as an indication.

[39] To check if our two-scale decomposition of the surface satisfies these constraints, we have computed the correlation length of the large and small scales. For a non-Gaussian autocovariance function we define the correlation length as the maximum distance beyond which the absolute value of the autocovariance function never exceeds $1/e = 1/2.718$ times its maximum value. The large- and small-scale autocovariance functions $\Gamma_L(x, y)$ and $\Gamma_R(x, y)$ have been computed as the inverse Fourier transform of their respective spectrum. Moreover, to avoid defining a correlation length for each direction in the horizontal plane, the spectrum has been assumed isotropic, i.e., $F(K, \alpha) = 1/2\pi$ in (41). This does not modify our conclusions. We used the spectrum presented by *Lemaire et al.* [1999] with the same values for the significant slope and the fetch as above. We considered the three wind friction velocity values 20 cm/s, 60 cm/s, and 100 cm/s and three frequencies 5.3 GHz, 13.6 GHz, and 36 GHz, for which we perform the comparisons between the BPM and the two-scale IEM in the section 4.

[40] The results confirm that condition (49) for the zeroth-order term is satisfied. For the first-order term, Figure 2 presents the computed couples $(k\sigma_R, kl_R)$

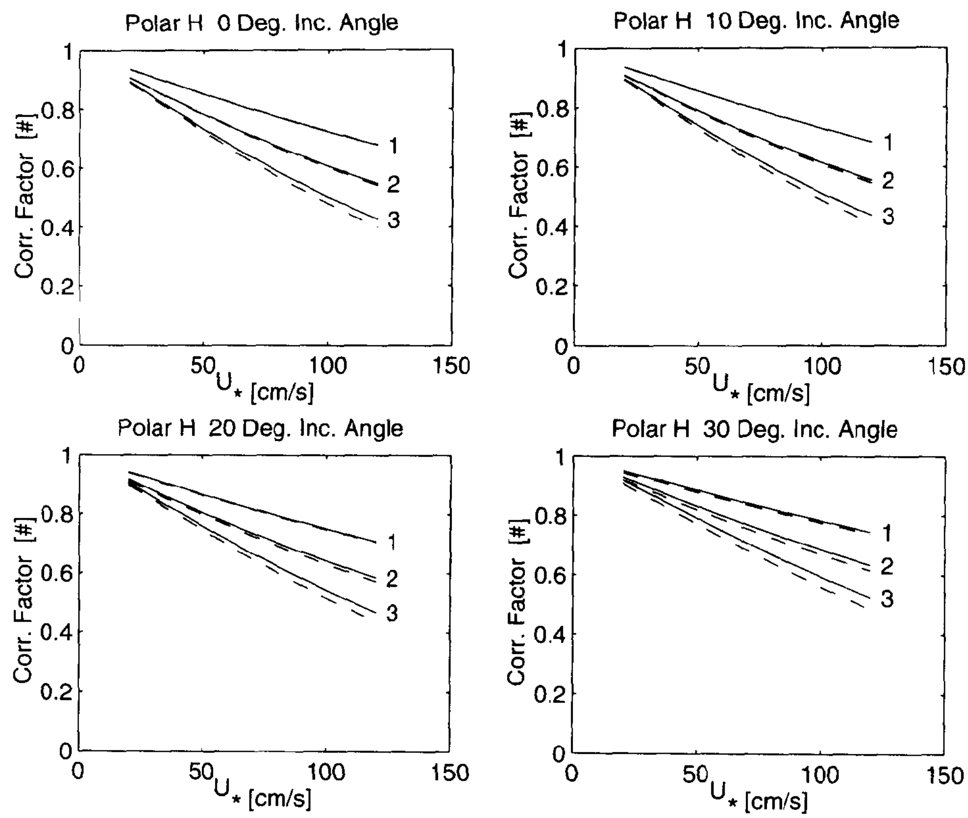


**Figure 3.** Correction factor $\alpha_{corr}$ to the Fresnel coefficient for HH polarization: BPM (solid lines) and IEM (dashed lines). Numbers 1, 2, and 3 stand for C, Ku, and Ka bands, respectively.

together with the limit of validity (50) expressed by *Thorsos and Jackson* [1989]. We note that in most configurations the couples ($k\sigma_R$, $kl_R$) are close to Thorsos and Jackson's limit. Since condition (50) was established for a rough surface with a one-dimensional (1-D) Gaussian spectrum and not for a natural surface such as the ocean (whose radial spectrum is close to a power law), we may not conclude that the proximity of ($k\sigma_R$, $kl_R$) to this limit implies that the contribution of terms higher than the first order to the total $\sigma^o$ will be negligible. Nevertheless, it does still indicate that their contribution should be small, as confirmed by the calculations (see section 4). Similarly, at high frequency, large wind friction velocity, and large incidence angle, the computed couple ($k\sigma_R$, $kl_R$) slightly departs from the limit expressed by Thorsos and Jackson, indicating that terms higher than the first order might be necessary for an accurate computation of the total scattering coefficient. Let us also mention that the computed values of the couples ($k\sigma_R$, $kl_R$) compare very well with the validity range computed by *Chen and Fung* [1988]. Finally, we also tested other spectra from the literature [*Bjerkaas and Riedel*, 1979; *Elfouhaily et al.*, 1997] with the same conclusions.

[41] These computations show that the proposed method for the two-scale decomposition of the surface provides a good compromise between the constraints expressed for each scale. Moreover, this method takes the roughness of the surface and the instrumental configuration into account for the computation of the limiting wave number and constitutes therefore an improvement compared to models in which $\delta = K_{\lim}/k$ is given an arbitrary fixed value.

## 4. Results

[42] Simulations have been performed for the case of the ocean surface using the BPM and the two-scale IEM. We considered a large range of incidence angles for three different frequencies (5.3 GHz, 13.6 GHz, and 36.0 GHz) and three incident-scattered polarization combinations (VV, HH, and VH). We used the ocean surface spectrum

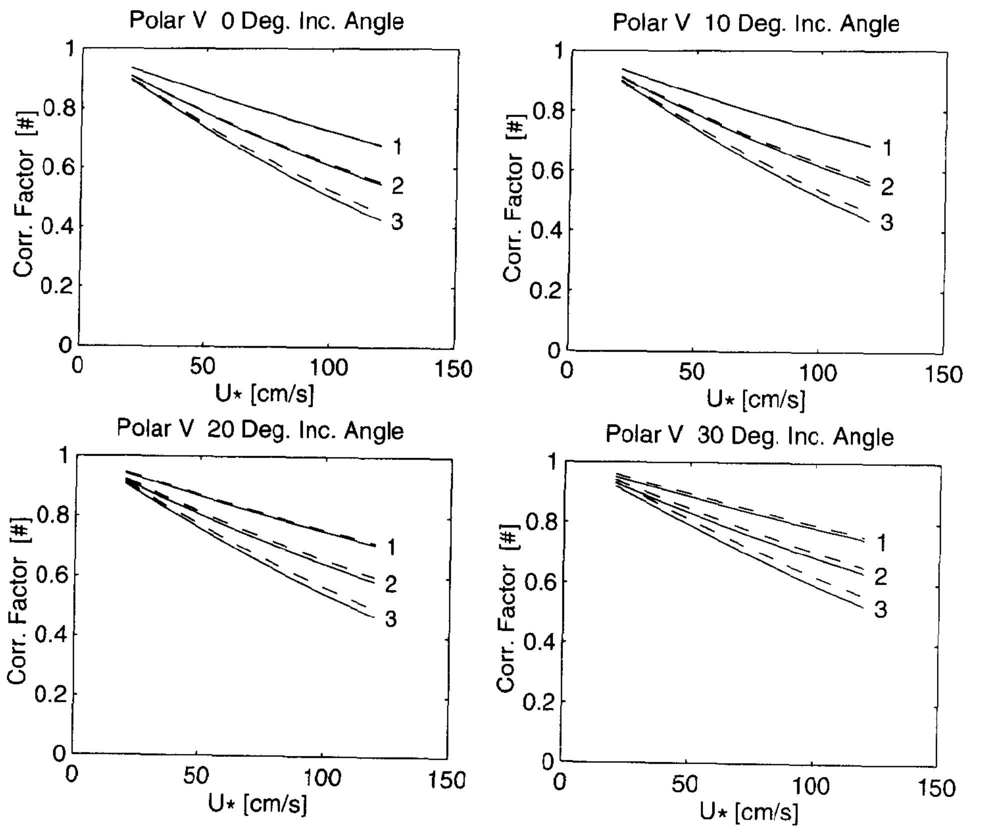


**Figure 4.** Correction factor $\alpha_{corr}$ to the Fresnel coefficient for VV polarization: BPM (solid lines) and IEM (dashed lines). Numbers 1, 2, and 3 stand for C, Ku, and Ka bands, respectively.

presented by *Lemaire et al.* [1999] with a fetch of 500 km and a significant slope equal to 0.70% as previously. Three different wind friction velocities have been considered: 20 cm/s, 60 cm/s, and 100 cm/s. For the large scale we used the *Cox and Munk* [1954a, 1954b] slope PDF, but with the slope variance computed from the surface spectrum. Finally, all simulations have been performed for a view angle aligned with the wind direction.

[43] First, we analyzed the difference between zeroth-order correcting factors for the Fresnel coefficient as expressed by (26) for the BPM and (32) for the IEM. The analysis has been performed for both HH and VV polarizations and for low incidence angles at which $\sigma^o_{pq0}$ is the dominant contribution to $\sigma^o_{pq}$. The results are presented in Figures 3 and 4, where we plotted the correction factor $\alpha_{corr}$ to the Fresnel coefficient, defined as

$$\alpha_{corr} = \frac{|R_{eff,pq}|^2}{|R_{pq}|^2}. \tag{51}$$

We note that there is no important difference between the two corrective coefficients. The maximum difference reaches a few tenths of a decibel for 30 deg. Since, for such incidence angle, $\sigma^o_{pq1}$ has the same order of magnitude as $\sigma^o_{pq0}$ (see Figures 8 and 9), this means an even lower difference on the total scattering coefficient. We conclude therefore that the exponential correction (26) is an excellent approximation of (32) and presents an advantage of computational efficiency since it avoids a two-dimensional integration.

[44] Next, we computed the total scattering coefficient using the BPM and the two-scale IEM (up to third order). The results are displayed in Figures 5, 6, and 7, where angular points in the curves are due to the fixed 10 deg increment in the incidence angle. The results of the simulations using the SPM are also displayed to show the importance of the tilting by large waves, i.e., the difference between the BPM and SPM curves.

[45] In most configurations the difference between the BPM and the two-scale IEM results is small, if not

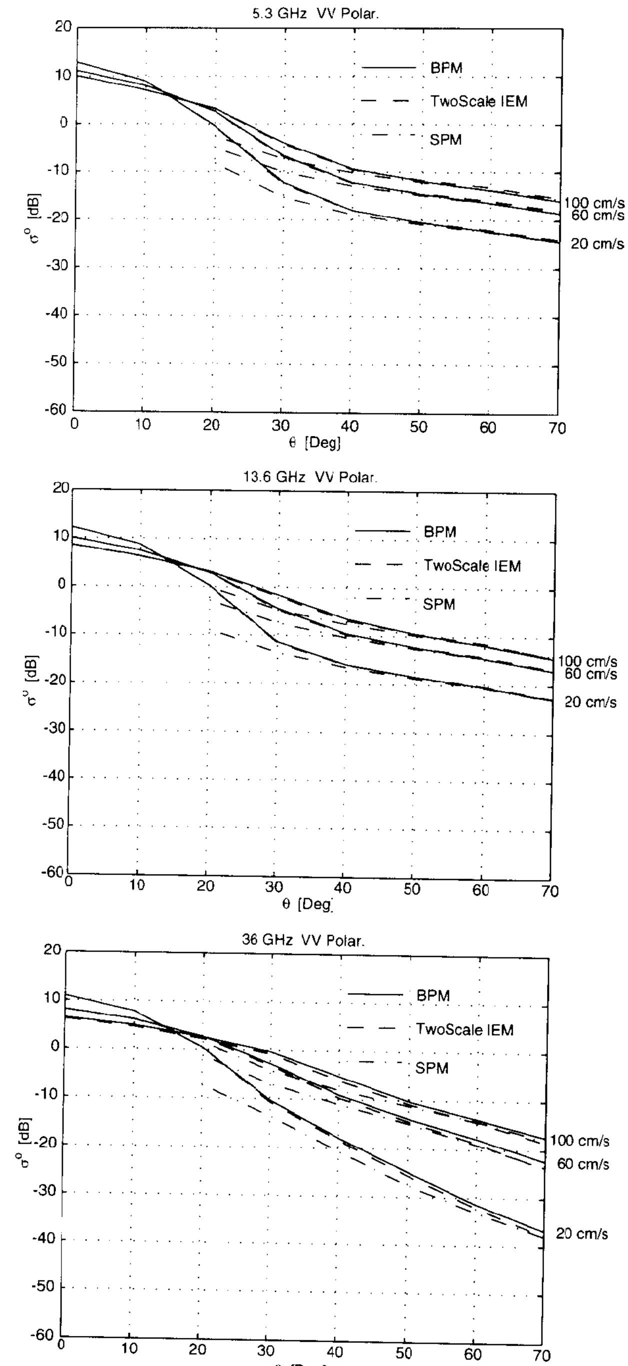


**Figure 5.** Comparison between BPM, IEM, and SPM models for backscattering case and VV polarization.

negligible, with regard to the accuracy of radar measurements. The largest differences occur at large incidence angle, large wind (i.e., important roughness), and high frequency, where it is of the order of 1 dB. The difference is also slightly larger in HH than in the other polarization configurations.

[46] As underlined at the end of section 2.3, the two-scale expansion of the IEM does not correspond

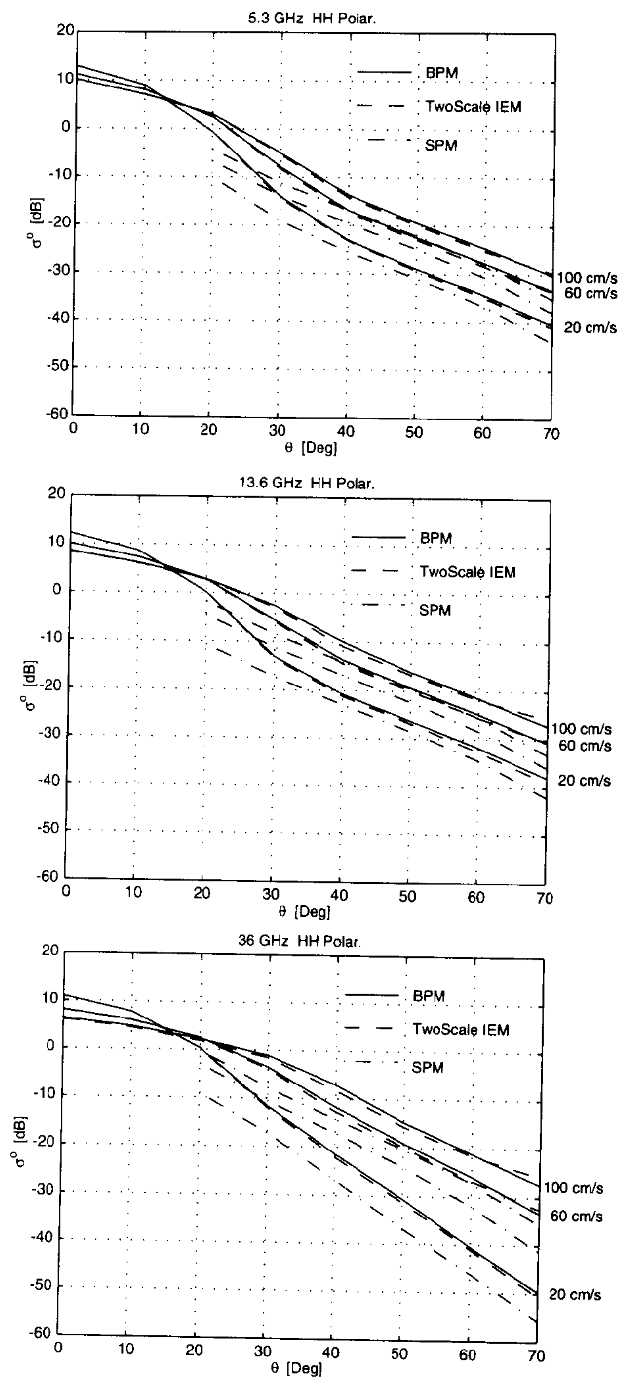


**Figure 6.** Comparison between BPM, IEM, and SPM models for backscattering case and HH polarization.

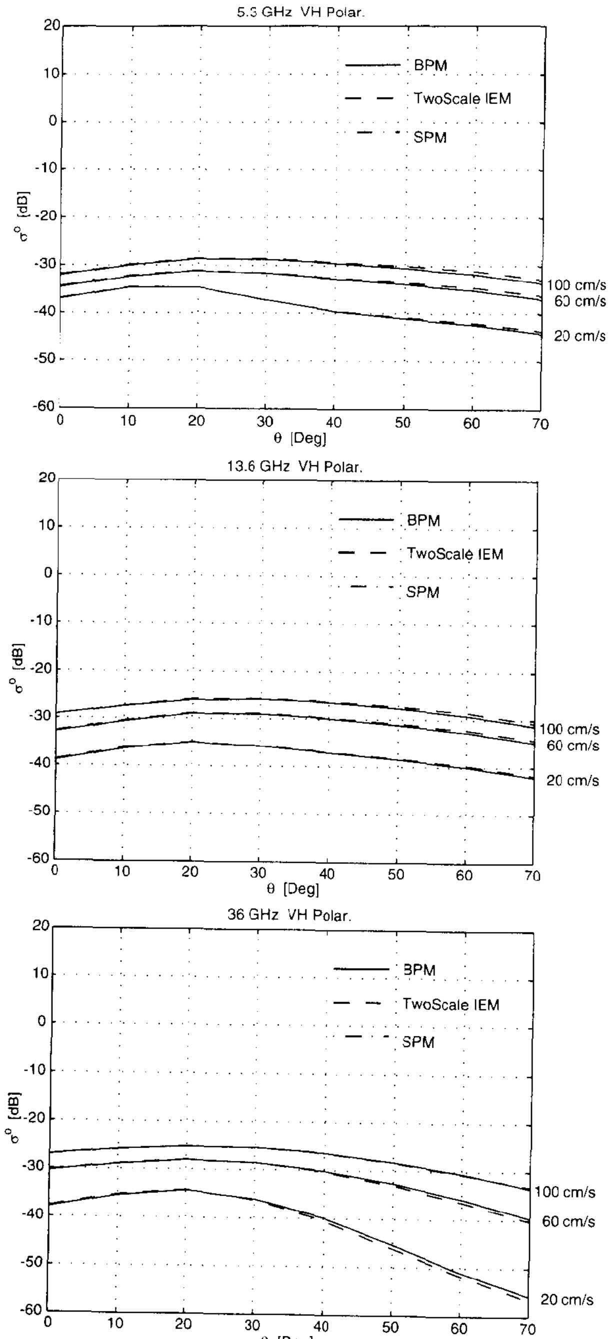


**Figure 7.** Comparison between BPM and IEM models for backscattering case and VH polarization. SPM reduces to $\sigma^o$ = 0 in this configuration.

exactly to the tilted Bragg solution, as the BPM does. The differences are (1) the use of global incidence angles for the vertical components of the incident and scattered wave number vectors and (2) the exponential factors $\exp\{-[\sigma^2 v_z{}^2]\}$ and $\exp\{-[\sigma^2 k_{iz}k_{sz}]\}$ in the expressions (36) and (38) of $\sigma^o_{pqn}$ and $I_{pqn}$, which do not appear in the tilted Bragg solution. It is therefore interesting to analyze the contribution of each term of the two-scale IEM.

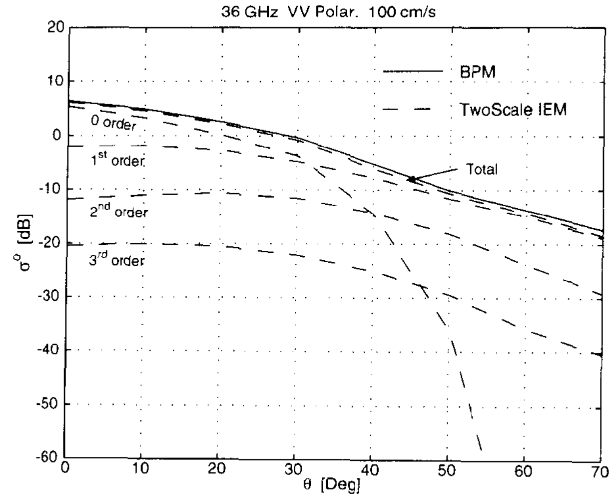


**Figure 8.** Successive terms of $\sigma^o$ using the two-scale IEM (36 GHz, VV polarization).

[47] Figures 8 and 9 present the results in VV and HH polarizations at 36 GHz and large wind friction velocity, i.e., for the configurations where the difference between the BPM and the two-scale IEM is the largest. Let us concentrate on the VV configuration first. We note that the difference between two $\sigma^o_{pqn}$ in successive orders (higher than the first) is roughly about 10 dB. This

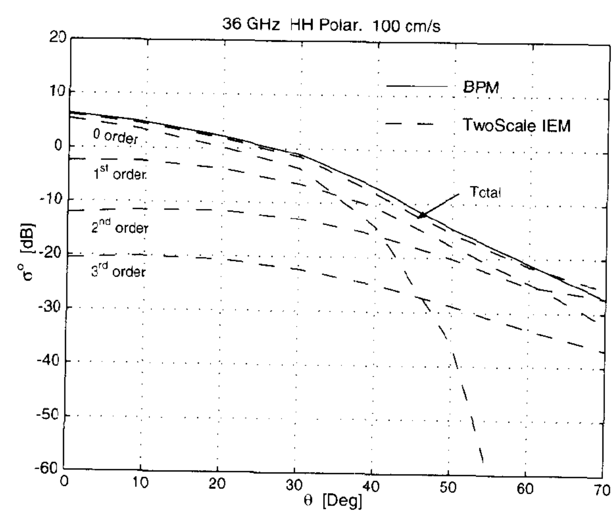


**Figure 9.** Successive terms of $\sigma^o$ using the two-scale IEM (36 GHz, HH polarization).